

# Light extraction and optical loss mechanisms in organic light-emitting diodes: Influence of the emitter quantum efficiency

Cite as: J. Appl. Phys. **104**, 123109 (2008); <https://doi.org/10.1063/1.3043800>

Submitted: 01 September 2008 . Accepted: 31 October 2008 . Published Online: 18 December 2008

Stefan Nowy, Benjamin C. Krummacher, Jörg Frischeisen, Nils A. Reinke, and Wolfgang Brütting



View Online



Export Citation

## ARTICLES YOU MAY BE INTERESTED IN

[Quantification of energy loss mechanisms in organic light-emitting diodes](#)

Applied Physics Letters **97**, 253305 (2010); <https://doi.org/10.1063/1.3527936>

[Determination of molecular dipole orientation in doped fluorescent organic thin films by photoluminescence measurements](#)

Applied Physics Letters **96**, 073302 (2010); <https://doi.org/10.1063/1.3309705>

[Nearly 100% internal phosphorescence efficiency in an organic light-emitting device](#)

Journal of Applied Physics **90**, 5048 (2001); <https://doi.org/10.1063/1.1409582>

Lock-in Amplifiers

... and more, from DC to 600 MHz



# Light extraction and optical loss mechanisms in organic light-emitting diodes: Influence of the emitter quantum efficiency

Stefan Nowy,<sup>1,a)</sup> Benjamin C. Krummacher,<sup>2</sup> Jörg Frischeisen,<sup>1</sup> Nils A. Reinke,<sup>1,b)</sup> and Wolfgang Brütting<sup>1,c)</sup>

<sup>1</sup>Experimental Physics IV, University of Augsburg, 86135 Augsburg, Germany

<sup>2</sup>OSRAM Opto Semiconductors, OLED-Lighting, Leibnizstr. 4, 93055 Regensburg, Germany

(Received 1 September 2008; accepted 31 October 2008; published online 18 December 2008)

The internal quantum efficiency of organic light-emitting diodes (OLEDs) can reach values close to 100% if phosphorescent emitters to harvest triplet excitons are used; however, the fraction of light that is actually leaving the device is considerably less. Loss mechanisms are, for example, waveguiding in the organic layers and the substrate as well as the excitation of surface plasmon polaritons at metallic electrodes. Additionally, absorption in the organic layers and the electrodes can play a role. In this work we use numerical simulations to identify and quantify different loss mechanisms. Changing simulation parameters, for example, the distance of the emitter material to the cathode or thicknesses of the various layers, enables us to study their influence on the fraction of light leaving the OLED. An important parameter in these simulations and for the actual device is the radiative quantum efficiency  $q$ , which is defined as the efficiency of radiative exciton decay in an unbounded space filled by the emitting dye and its matrix. The simulations show that due to microcavity effects the radiative decay channel can be considerably changed in an OLED as compared to free space emission of a dipole. Thus the knowledge of the radiative quantum efficiency is crucial for the optimization of OLEDs. As an example, we present simulations of bottom-emitting OLEDs based on the well-known green emitter tris-(8-hydroxyquinoline) aluminum with transparent indium tin oxide anode and a calcium/aluminum cathode. © 2008 American Institute of Physics. [DOI: 10.1063/1.3043800]

## I. INTRODUCTION

Organic semiconductors have found important applications as active materials in organic light-emitting diodes (OLEDs). Owing to a vast amount of both fundamental and device oriented studies, their principal working mechanisms have been clarified. However, concerning the efficiency of converting electrical power into emitted photons, they still need to be improved further in order to compete with established lighting technologies.

Traditionally, the external quantum efficiency  $\eta_{\text{EQE}}$ , i.e., the number of photons emitted from the OLED per charge carriers injected into the device, is given by the product of four different factors,<sup>1</sup>

$$\eta_{\text{EQE}} = \gamma \times \eta_{s/t} \times q \times \eta_{\text{out}}. \quad (1)$$

Therein,  $\gamma$  is the charge balance factor,  $\eta_{s/t}$  is the singlet/triplet ratio,  $q$  is the radiative quantum efficiency of the emitter material, and  $\eta_{\text{out}}$  is the outcoupling factor. It was demonstrated already in the pioneering work of Tang and VanSlyke<sup>2</sup> that  $\gamma$  can be brought close to one in heterolayer structures. Another important step was the introduction of phosphorescent emitters by Baldo *et al.*<sup>3</sup> Many subsequent studies have established that for fluorescent emitters one can assume  $\eta_{s/t}=0.25$  and for phosphorescent emitters  $\eta_{s/t}=1$ .

Thus the product  $\gamma \times \eta_{s/t}$  gives the fraction of injected carriers forming excitons that are in principle able to generate radiation inside an OLED. Their fate is determined by the remaining two factors  $q \times \eta_{\text{out}}$ . Quantifying both of them is the subject of the optical simulations described in this paper. Originally,  $q$  was taken to be the photoluminescence (PL) quantum efficiency of the emitter material in an unbounded medium. However, it has been realized by various authors that the radiative decay rates of fluorescent dyes close to a metal electrode or embedded in the microcavity of an OLED can be significantly different as compared to the free-space values.<sup>4–8</sup> Thus the determination of the remaining extraction efficiency  $\eta_{\text{out}}$  of radiation generated inside the OLED multilayer structure to the outside world is not straightforward. As a crude approximation,  $\eta_{\text{out}}$  can be estimated as  $1/(2n^2)$  for isotropic emitters, where  $n$  is the refractive index of the emitting organic layer.<sup>9</sup> However, in detail this value depends on the composition of the OLED stack as well as the position and the orientation of the emitting molecules inside the structure.<sup>10,11</sup> Thus for both, answering fundamental questions, such as the singlet-triplet ratio and a focused device optimization, quantitative knowledge of the radiative quantum efficiency and the light-outcoupling factor are required.

In this paper, we will use optical simulations to quantify light extraction and optical loss channels in OLEDs. After presenting the basic physics behind the model, we will first show for a simple model OLED based on tris-(8-hydroxyquinoline) aluminum (Alq<sub>3</sub>) as fluorescent emitting

<sup>a)</sup>Electronic mail: stefan.nowy@physik.uni-augsburg.de.

<sup>b)</sup>Present address: Institute for Computational Physics, Zurich University of Applied Sciences, P.O. Box 805, 8401 Winterthur, Switzerland.

<sup>c)</sup>Electronic mail: wolfgang.brueetting@physik.uni-augsburg.de.

Al	100 nm
Ca	15 nm
Alq <sub>3</sub>	80 nm
TPD	80 nm
PEDOT:PSS	30 nm
ITO	140 nm
glass	

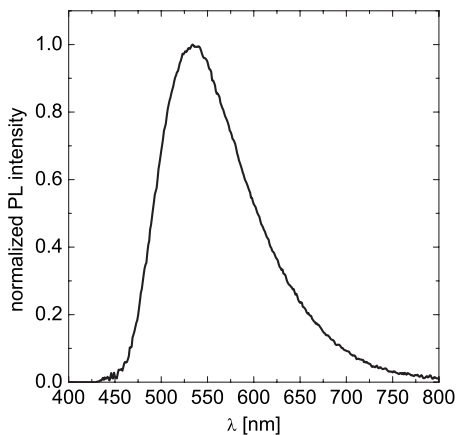
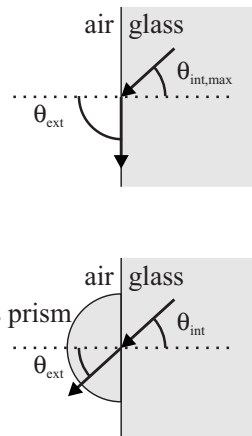
FIG. 1. Bottom-emitting OLED stack with transparent ITO anode.

material that the simulations comply very well with measured angular and polarization dependent emission spectra. We will furthermore demonstrate the influence of microcavity effects inside the OLED on the radiative quantum efficiency and finally quantify the influence of various device parameters on the amount of radiation going into different optical channels of an OLED. In a subsequent paper, we use optical simulations on a series of thickness variations in a phosphorescent OLED stack in order to determine the radiative quantum efficiency of the emitter material and thus demonstrate that the knowledge of this quantity is crucial for the optimization of the OLED design.<sup>12</sup>

## II. EXPERIMENTAL

The substrates for the bottom-emitting OLEDs (Fig. 1) consist of glass with a prestructured 140 nm thick indium tin oxide (ITO) layer. A 30 nm thin layer of poly(3,4)-ethylenedioxythiophene doped with poly(styrene sulfonate) (PEDOT:PSS) is spin cast onto the substrate and dried on a hot plate. All following organic and metal layers are deposited through shadow masks in a high vacuum chamber (base pressure  $<3 \times 10^{-7}$  mbar) without breaking the vacuum. Organic materials are deposited using effusion cells. As hole transporter *N,N'*-diphenyl-*N,N'*-bis(3-methylphenyl)-1,1'-biphenyl-4,4'-diamine (TPD) with a thickness of 80 nm is used. The emitter is Alq<sub>3</sub> with a thickness of 80 nm, which has a PL peak emission of about 535 nm (Fig. 2). As cathode, deposited by thermal evaporation, aluminum on top of calcium is used.

After evaporation current-voltage (*I-V*) and luminance-voltage (*L-V*) characteristics of the OLEDs are recorded simultaneously in a glovebox system under dry N<sub>2</sub> atmosphere

FIG. 2. PL spectrum of Alq<sub>3</sub>.FIG. 3. Maximum internal angle for glass/air interface  $\theta_{\text{int,max}} \approx 41^\circ$  (top) and the case for attached semicircle prism:  $\theta_{\text{int}} = \theta_{\text{ext}}$  (bottom).

to find the working point of the devices. Before taking the samples out to ambient air, they are encapsulated with a glass slide and epoxy glue.

The angular emission spectrum of an OLED is recorded with a calibrated charge coupled device spectrometer. The OLED is placed on a computer controlled rotary stage. Light emitted at a given angle is focused by a collimator lens and coupled into an optical fiber, which leads to the spectrometer. Furthermore a semicircle prism can be attached to the OLED's glass substrate by applying an optical gel. Compared to the spectrum without the prism this additionally allows the study of light, which normally is guided in the substrate (Fig. 3). Without the prism this light cannot leave the substrate directly due to total internal reflection caused by the difference in the refractive indices of the glass/air interface ( $n_{\text{glass}} \approx 1.52$ ,  $n_{\text{air}} = 1$ ).

## III. SIMULATION METHOD

The design of OLEDs must consider near field phenomena and the photonic mode density due to the use of thin organic films.<sup>11</sup> The traditional approach for device simulations is the dipole model, which finds its basis in an early paper by Sommerfeld,<sup>13</sup> where the propagation of radio-waves above the Earth's conducting surface was investigated. Later Chance, Prock, and Silbey (CPS)<sup>5,6</sup> adapted this model for molecular fluorescence and energy transfer near interfaces. This model was extended to the near-field optics of OLEDs by various authors,<sup>10,11,14-16</sup> where an exciton within the OLED is modeled as a point dipole driven by the reflected electromagnetic waves inside a microcavity.

The simulations presented in this work are also based on this traditional CPS approach of emissive dipoles. The dipoles, embedded in the multilayer stack of an OLED, are treated as forced damped harmonic oscillators<sup>11</sup>

$$\frac{d^2 p}{dt^2} + \omega_0^2 p = \frac{e^2}{m} E_r - b_0 \frac{dp}{dt}, \quad (2)$$

where  $p$  is the electric dipole moment,  $\omega_0$  is the resonant angular frequency in the absence of damping,  $m$  is the effective mass,  $e$  is the electric charge,  $E_r$  is the reflected electric field at the dipole position, and  $b_0$  is the radiative decay rate

(or damping constant) in the absence of any interfaces. Both the dipole and the reflected field oscillate with the same complex frequency  $\Omega = \omega - ib/2$  as

$$p = p_0 \exp(-i\Omega t) \quad \text{and} \quad E_r = E_0 \exp(-i\Omega t), \quad (3)$$

where  $\omega$  and  $b$  are the frequency and decay rate in the presence of the interface. Then the modified decay rate is obtained as

$$b = b_0 + \frac{e^2}{m\omega p_0} \text{Im}(E_0). \quad (4)$$

The difference in frequency is usually quite small and will not be considered here.<sup>11</sup> This equation shows that the change in the decay rate is determined by the magnitude of the reflected electric field at the position of the emitting dipole. It is calculated using the Hertz vector and solving the Helmholtz equation by an expansion of the field in plane waves (for details see, e.g., Lukosz and Kunz<sup>17</sup>). Thereby all layers in this multilayer stack are treated as infinite in two dimensions, having a certain thickness in the third direction. The interface between two layers is assumed sharp and without roughness. Using a transfer matrix method the Fresnel coefficients are calculated by taking the optical constants and thicknesses of the different layers of the OLED stack into account, as well as the position of the dipoles within the OLED, which is assumed to be sharp as well. The modified decay rate for arbitrary dipole orientation can then be expressed as a combination of parallel and perpendicular contributions  $b_{\parallel}$  and  $b_{\perp}$ , respectively, which are calculated numerically by integrating over all in-plane wave vector values of  $k_x$  from 0 to  $\infty$  using the Fresnel coefficients for  $s$ - and  $p$ -polarized light [for details see CPS (Ref. 6) or Barnes<sup>11</sup>]. Finally the orientation of the dipoles (parallel or perpendicular to the substrate, weighed 2:1 for isotropic dipole orientation) yielding

$$b_{\text{iso}} = \frac{2}{3}b_{\parallel} + \frac{1}{3}b_{\perp} \quad (5)$$

and the emission spectrum of the emitter is taken into account. As a result we obtain a polychromatic power dissipation spectrum, i.e., the contribution of modes with in-plane wave vector component  $k_x$  to the spontaneous emission decay rate of the dipoles at each wavelength (see e.g., Fig. 4). The concept of in-plane wave vectors is very useful: it not only describes light traveling under a certain angle in a layer of the OLED, it also is conserved at interfaces between different layers. Furthermore high values of  $k_x > (2\pi/\lambda)n_{\text{glass}}$  represent nonemissive modes [waveguided modes and surface plasmon polaritons (SPPs)], which are near-field phenomena that are not described by ordinary plane waves for far field radiation.

Comparing our simulation tool to the calculations from different groups in literature,<sup>18,19</sup> we can confirm their basic findings, which strengthens the confidence for our tool. There are, however, several other possibilities to simulate the emission spectra of OLEDs, but these do not grant access to the nonradiative modes and often are limited to specific stack types such as microcavities.<sup>20–22</sup> We would like to point out again that our simulations are polychromatic calculations using the full visible wavelength range and the optical con-

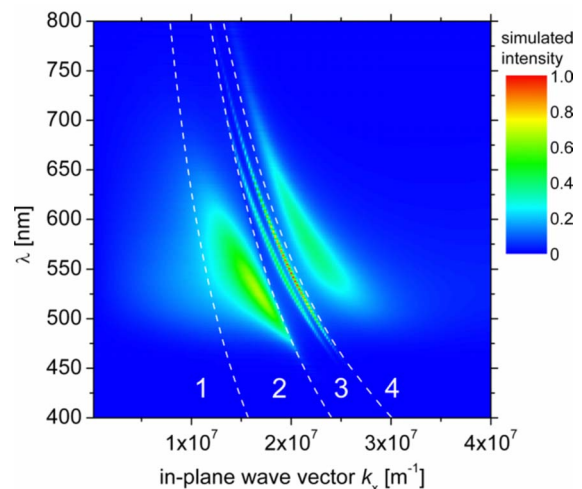


FIG. 4. (Color online) Power dissipation spectrum of an ITO OLED (Fig. 1): (1) light emitted directly from the OLED, (2) light trapped inside substrate, (3) waveguided modes, and (4) plasmons (SPPs).

stants for all layers from 400 to 800 nm. The optical constants were obtained by ellipsometric measurements for every material incorporated in the OLED stack. In the range of the Alq<sub>3</sub> emission (450–700 nm) the refractive index  $n$  varies between 1.53 and 1.51 for BK7, 2.02, and 1.82 for ITO, 1.61 and 1.56 for PEDOT:PSS, 1.80 and 1.68 for TPD, 1.81 and 1.69 for Alq<sub>3</sub>, 0.50 and 0.65 for Ca, and 0.49 and 1.48 for Al. For all organic materials the extinction coefficient  $k$  is below 0.06 in this wavelength range, whereas it varies between 1.69 and 2.79 for Ca and between 4.60 and 6.98 for Al.

## IV. SIMULATION RESULTS

### A. Power dissipation spectra and mode analysis

As a first application of our simulation method we have calculated the power dissipation spectra of the well-known heterostructure OLED displayed in Fig. 1. Figure 4 shows a color-coded plot of the radiation as a function of wavelength  $\lambda$  and in-plane wave vector component  $k_x$ . Thereby the emission zone (dipole layer) is assumed to be infinitely thin and located at the interface between the hole and the electron transport material, and the orientation of the emitting molecules is taken to be isotropic. The underlying spectral weighting function is the PL spectrum of Alq<sub>3</sub> as the emitter material (Fig. 2). Furthermore, the radiative quantum efficiency of Alq<sub>3</sub> is taken to be 20%, i.e., equal to the PL quantum efficiency determined independently by us.<sup>23,24</sup> We note that higher values have been reported in literature,<sup>25,26</sup> however, this is not essential in the context of this work.

The power dissipation spectra can be split up into four regions. Region 1  $k_x < (2\pi/\lambda)n_{\text{air}}$  represents the light, which can leave the OLED directly (direct emission). Region 2  $(2\pi/\lambda)n_{\text{air}} < k_x < (2\pi/\lambda)n_{\text{glass}}$  denotes the amount of light, which is emitted to the glass substrate and is trapped there due to total internal reflection (emission to substrate). This fraction is accessible only if outcoupling structures such as prisms, lenses, or light-scattering foils are used, for examples see Meerholz and Müller.<sup>27</sup> For even larger values of  $k_x$  the

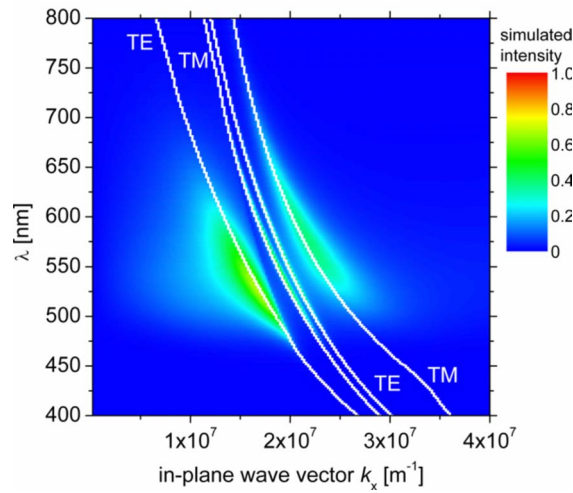


FIG. 5. (Color online) Same power dissipation spectrum as Fig. 4: identification of TE and TM modes. Waveguided modes and plasmons are located in regions 3 and 4, respectively.

radiation of the dipoles does no longer reach the glass substrate but is waveguided in the organic layers and the adjacent ITO electrode (waveguiding, region 3). Finally, for  $k_x > (2\pi/\lambda)n_{\text{ITO+organic}}$ , where  $n_{\text{ITO+organic}}$  denotes an effective refractive index of the ITO and organic layers taken together, the emitting dipoles couple to SPPs traveling at the organic-cathode interface (plasmons, region 4).

We note that for very small distances between the emitting dipoles and the metal electrodes ( $\leq 25$  nm) Förster-type coupling to lossy surface waves in the metal becomes important.<sup>11,16</sup> In contrast to SPPs, they do not enhance but decrease the spontaneous emission decay rate. However, as in practical OLEDs the emitter-to-metal distances are typically larger than this value, we do not make this distinction here and denote all contributions in region 4 as SPPs.

The identification of transverse electric (TE) and transverse magnetic (TM) modes shown in Fig. 5 uses a transfer matrix method, which is based on a three-layer waveguide calculation.<sup>28</sup> After considering the values of the in-plane wave vector  $k_x$ , the waveguided modes and the plasmons (the latter having always TM polarization) can be clearly identified. It is further seen that the mode traveling in the glass substrate has TE polarization. A cross section at  $\lambda = 525$  nm shown in Fig. 6 gives an impression of the relative strength of different contributions near the emission maximum of Alq<sub>3</sub>. Integrating over the different regions in the polychromatic power dissipation spectrum leads to the amount of power coupled into the different modes. For the OLED presented in Fig. 1 we obtain light emitted directly (4.2%), light emitted to the substrate (6.3%), waveguided modes (3.0%), plasmons (9.5%), absorption (3.3%), and all other (intrinsic nonradiative) losses (73.6%). Keeping in mind that Alq<sub>3</sub> is a singlet emitter, the numbers have to be multiplied by a factor of 1/4 in order to obtain the conversion efficiency of charge carriers into light, e.g., resulting in an external quantum efficiency of about 1% (only direct emission) for this OLED, which is in good agreement with the published results.<sup>2,29</sup> The value of the intrinsic nonradiative losses of 73.6% also deserves some comment. Starting with a

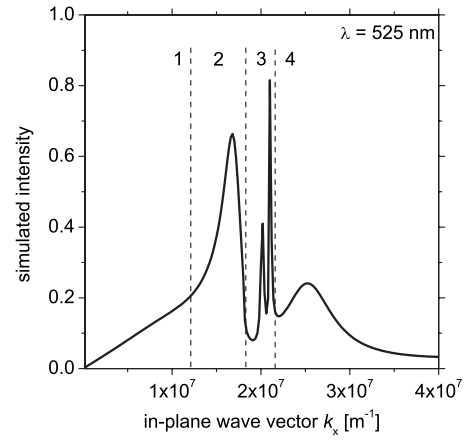


FIG. 6. Cross section in Fig. 5 at  $\lambda = 525$  nm: (1) light emitted directly, (2) light trapped inside substrate, (3) two sharp waveguided modes, and (4) a SPP.

fluorescence efficiency of 20%, one would expect this value to be exactly 80%; however, as will be discussed in detail in Sec. IV C, the presence of microcavity effects in an OLED modifies this value toward higher radiative rates of the emitting molecules.

## B. Comparison of experimental and simulated OLED emission spectra

To confirm the outcome of the simulations the power dissipation spectra are transformed and compared to the experimental angular emission spectra of the OLED, optionally with determination of *s*- and *p*-polarization. Therefore the external angle of emission  $\theta_{\text{ext}}$  is calculated from the in-plane wave vector component  $k_x$ ,

$$\theta_{\text{ext}}(k_x, \lambda) = \arcsin\left(\frac{k_x}{k(n(\lambda), \lambda)}\right) = \arcsin\left(\frac{k_x}{2\pi n(\lambda)}\lambda\right). \quad (6)$$

Therein  $\lambda$  is the vacuum wavelength of the light,  $n(\lambda)$  is the refractive index either of air for light emitted directly from the device [ $n(\lambda) = n_{\text{air}}$ ] or it is the refractive index of the glass substrate for light trapped inside the substrate [ $n(\lambda) = n_{\text{glass}}(\lambda)$ ]. The measured angular emission spectra of the ITO OLED (already presented in Fig. 1) are shown in Fig. 7 with distinction of *s*- and *p*-polarized light emission and compared to the simulation results.

These spectra are in very good agreement concerning the angular characteristics. The spectral pattern is slightly broadened at longer wavelengths in the simulation; this might be due to a too broad PL spectrum of Alq<sub>3</sub> used in the simulations. Both simulation and experiment show the maximum emission perpendicular to the substrate ( $\theta_{\text{ext}} = 0^\circ$ ). The decrease in the emission intensity at higher angles  $\theta_{\text{ext}}$  follows Lambert's cosine law. Since the emission pattern is changing very little with the angle  $\theta_{\text{ext}}$ , the device's color stability is very good. Light emitted from this ITO device is mainly unpolarized since the *s*-polarized and *p*-polarized spectra differ only very little.

Figure 8 shows the same device with a semicircle prism attached to the glass substrate. Here again the simulated spectra are in good agreement with the experiment. Compari-

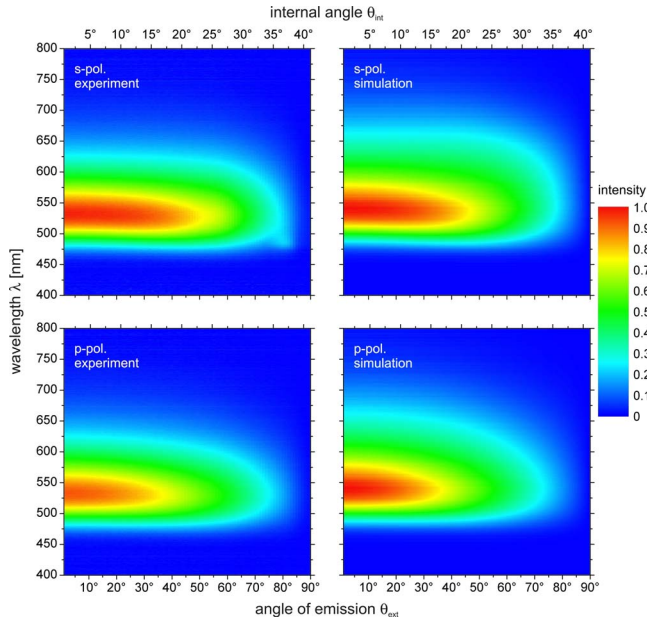


FIG. 7. (Color online) *s*- and *p*-polarized angular emission spectra of the ITO OLED shown in Fig. 1. The top *x*-axis shows the internal angle calculated for the glass substrate with a refractive index of  $n_{\text{glass}} \approx 1.52$ . Please note that the actual refractive index of the BK7 substrate is wavelength dependent and therefore the internal angle slightly differs for different wavelengths.

son of these results to the OLED with planar substrate (Fig. 7) shows that in the latter a considerable amount of radiation is trapped inside the glass substrate. As the intensity of light emitted normal to the substrate is the same for both cases (with and without prism), there is actually a big portion of light emitted at large angles; the peak intensity at about  $\theta_{\text{ext}} \approx 65^\circ$  is almost two times higher than the peak intensity of the perpendicular emission. Please note that the figures are normalized with respect to the highest intensity obtained in

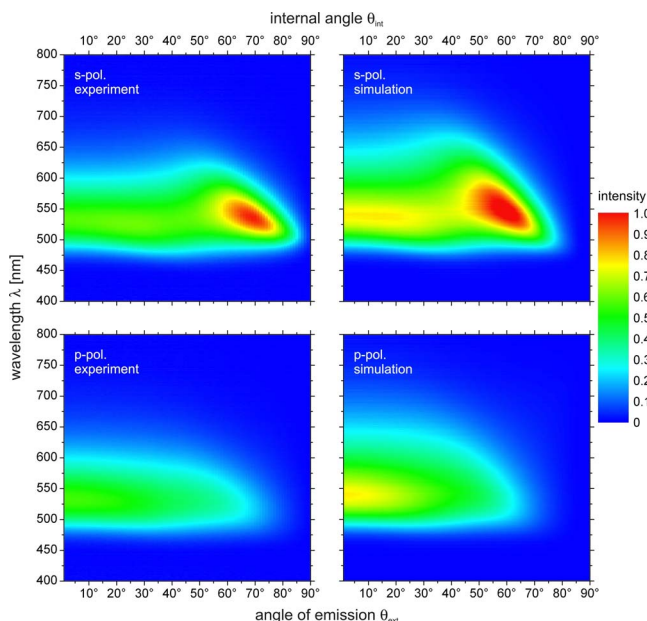


FIG. 8. (Color online) *s*- and *p*-polarized angular emission spectra of the ITO OLED shown in Fig. 1 with attached semicircle prism (no internal total reflection at the glass/air interface).

each of them except that corresponding *s*- and *p*-polarized spectra are normalized with the same factor. The difference in *s*- and *p*-polarized emission shows that the substrate-guided light is *s*-polarized, which is consistent with the simulation and the identification of modes in Fig. 5. So after attaching an outcoupling structure to the OLED substrate, an *s*-polarized leaky mode is emitted, having a slight dispersion in the wavelength.

We note that there is a very good agreement between simulation and experiment, also for microcavity devices with two metallic electrodes. However this is not shown here and has been reported elsewhere.<sup>30</sup>

### C. Microcavity effects on the internal quantum efficiency of OLEDs

The radiative quantum efficiency  $q$ , which is defined as the efficiency of radiative decay of the emitter material in an unbounded space filled by the dye and its matrix, is a crucial factor in our simulation, as it handles any nonradiative decay of the emitting dipoles,

$$q = \frac{k_r}{k_r + \sum k_{nr}}, \quad (7)$$

where  $k_r$  is the radiative decay rate and  $\sum k_{nr}$  denotes the sum of the decay rates of all competing processes. In the work of Smith *et al.*,<sup>15</sup> effects of a quantum efficiency smaller than 100% have been discussed; however, the impact on the simulation and device optimization of OLEDs has not been investigated in detail.

The effect of the radiative quantum efficiency  $q$  on the external quantum efficiency  $\eta_{\text{EQE}}$  of the OLED can be described by the following equation:

$$\eta_{\text{EQE}} = \gamma \times \eta_{s/t} \times q_{\text{eff}}(q) \times \eta_{\text{out}}, \quad (8)$$

where, as before,  $\gamma$  is the charge balance factor,  $\eta_{s/t}$  is the singlet/triplet ratio (for fluorescent emitters we assume  $\eta_{s/t} = 0.25$  and for phosphorescent emitters  $\eta_{s/t} = 1$ ), and  $\eta_{\text{out}}$  is the outcoupling factor. The presence of a cavity, for example, due to the electrodes in an OLED, influences the lifetime of the radiative dipoles.<sup>5,6,8</sup> This means that the radiative decay channel of the dipoles can be attenuated or enhanced due to the surrounding material of the dipole or the presence of interfaces, in particular to metals. As a consequence the radiative quantum efficiency  $q$  has to be replaced by an effective quantum efficiency  $q_{\text{eff}}$  (depending on  $q$ ), which has the consequence that for a given (experimentally determined) value of the external quantum efficiency  $\eta_{\text{EQE}}$  of an OLED the outcoupling factor  $\eta_{\text{out}}$  will change too. We therefore define  $q_{\text{eff}}$  as the radiative quantum efficiency of an excited molecule due to the presence of the cavity,

$$q_{\text{eff}} = \frac{k_r^*}{k_r^* + \sum k_{nr}}, \quad (9)$$

where  $k_r^*$  is the radiative decay rate determined by the boundary conditions of the electromagnetic field in the optical cavity. Please note that  $q_{\text{eff}}$  is specific for a given stack structure,

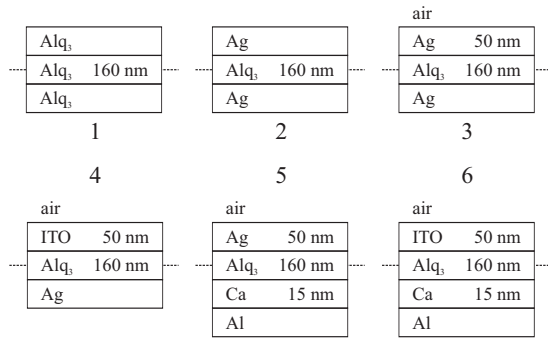


FIG. 9. Sample stacks for the illustration of  $q_{\text{eff}}$ . Layers without thickness specification are assumed to be semi-infinite. The emissive dipoles are located in the middle of the Alq<sub>3</sub> layer as a  $\delta$ -distribution.

its layer thicknesses, and the distance of the dipoles to interfaces.

To demonstrate the effect of the cavity on  $q_{\text{eff}}$ , we have performed simulations on some simple model structures (Fig. 9), comprising Alq<sub>3</sub> (assumed for simplicity to be non-absorbing) as the emitter and different electrodes (Ag, ITO, and Ca/Al). The obtained fractions of radiation going into different channels are listed together with the values for  $q_{\text{eff}}$ ,  $1 - q_{\text{eff}}$  (effective nonradiative losses), and  $\eta_{\text{out}}$  in Table I. (Please note that the *total emission* is the sum of the *direct emission* and the *emission to substrate*.) Values of  $q_{\text{eff}}$  larger than the assumed quantum efficiency  $q=0.20$  indicate that due to the presence of the cavity the emission of the dipole is accelerated.  $\eta_{\text{out}}$  is calculated as the fraction of the total emission and  $q_{\text{eff}}$ .

As Alq<sub>3</sub> is set to be nonabsorbing, device 1 (corresponding to dipoles embedded in an infinitely thick Alq<sub>3</sub> layer) shows no absorption at all and obviously no waveguide modes and surface plasmons can be excited. Since there is no cavity, the dipole does not get accelerated and the effective quantum efficiency is equal to the radiative quantum efficiency ( $q_{\text{eff}}=q=0.20$ ). Device 2 represents a strong cavity, where the Alq<sub>3</sub> layer is embedded between two Ag electrodes. As these are semi-infinite no light can be emitted from this device. However the amplification of the dipole is expressed in an increased  $q_{\text{eff}}$  of 0.34. So in principle this silver cavity device could have an increased light output. This enhancement of  $q_{\text{eff}}$  can be used in the next step (device 3). Here one of the Ag layers is only 50 nm thick, which in principle allows light to be coupled out to air. The effective quantum efficiency is unchanged compared to device 2. However, still only 1% of the power is emitted as light; this

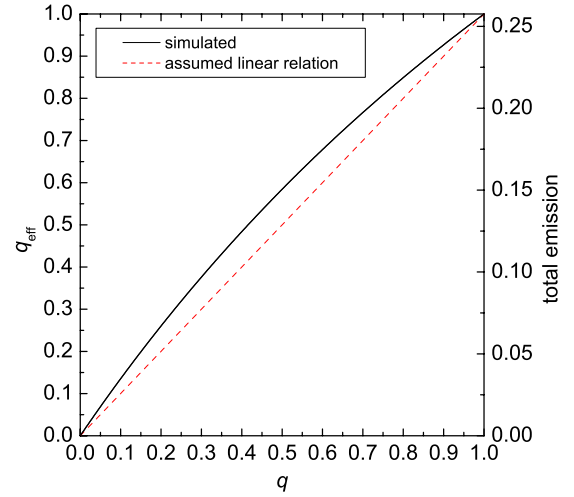


FIG. 10. (Color online) Solid black curve: relation between the radiative quantum efficiency  $q$  and the effective quantum efficiency  $q_{\text{eff}}$  for device 4 (left axis) and simulated fraction of power of the total emission (right axis). Dashed red curve: assumed linear dependence between  $q$  and  $q_{\text{eff}}$  (left axis) and the fraction of power of the total emission (right axis), respectively.

could be increased with a more transparent electrode. This can be seen for device 4, where the thin Ag electrode is substituted with an ITO layer. The fraction of emitted light reaches 7%, however, ITO shows a weaker microcavity effect as compared to the silver electrode. This effect explains the smaller value of  $q_{\text{eff}}$ , when comparing device 4 with device 3. Finally, the thick silver electrode is substituted with a Ca/Al electrode. Both devices 5 and 6 have similar values as their counterparts 3 and 4, respectively. This means that the Ca/Al electrode is only slightly less effective in optical terms and could be used for some material systems, where it might be a better solution for the charge carrier injection than a Ag electrode.

At this point we would like to note that the relation between the radiative quantum efficiency  $q$  and the effective quantum efficiency  $q_{\text{eff}}$  is not just a linear factor ( $q_{\text{eff}} \neq q \times \text{const}$ ). This is illustrated in Fig. 10, which shows the relation between  $q$ , which is an input parameter for our simulations, and  $q_{\text{eff}}$  (which is determined by the simulation) for device 4 (left axis). The right axis in Fig. 10 shows the fraction of the total emitted power versus  $q$ . To guide the eye, a linear relation between  $q_{\text{eff}}$  and  $q$  is included in the figure. What can be seen clearly is a nonlinear enhancement being largest (in absolute values) at  $q \approx 0.5$ .

TABLE I. Calculation of  $q_{\text{eff}}$  for the model stacks in Fig. 9. Alq<sub>3</sub> is assumed to be nonabsorbing,  $q=0.20$ . If  $q_{\text{eff}} > q$  then the emission of the dipole is amplified.

Device	Total emission (%)	Waveguiding (%)	Plasmons (%)	Absorption (%)	$q_{\text{eff}}$	$1 - q_{\text{eff}}$	$\eta_{\text{out}}$ (%)
1	20.0	0.0	0.0	0.0	0.20	0.80	100
2	0.0	15.5	10.3	7.9	0.34	0.66	0.0
3	1.0	15.3	10.4	6.8	0.34	0.66	3.0
4	6.7	9.5	9.6	0.2	0.26	0.74	25.8
5	0.3	14.0	11.1	7.4	0.33	0.67	0.9
6	5.9	9.9	8.4	1.4	0.26	0.74	23.0

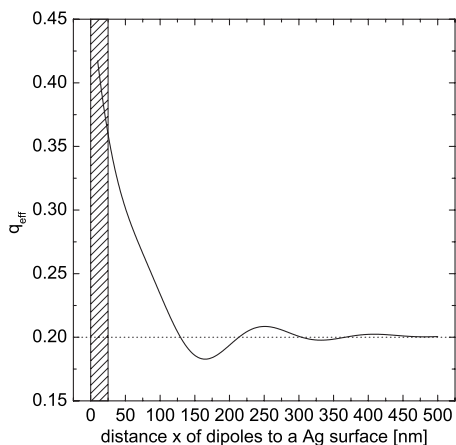


FIG. 11. Effective quantum efficiency  $q_{\text{eff}}$  as a function of the distance of dipoles to a silver surface. Radiative quantum efficiency  $q=0.20$ . The dipoles are residing in  $\text{Alq}_3$ . Very short distances of the dipoles to the Ag surface (hatched area): quenching effects.

Also, as mentioned before,  $q_{\text{eff}}$  is specific for a given stack type, its layer thicknesses, and the dipole position within it. Figure 11 shows the strong dependence of  $q_{\text{eff}}$  on the distance of the dipoles to a silver surface. For this and all the following simulations the absorption of  $\text{Alq}_3$  is incorporated. The dipoles reside in  $\text{Alq}_3$ , the radiative quantum efficiency is again set to  $q=0.20$ . What can be seen is that  $q_{\text{eff}}$  oscillates around the value of  $q$ ; however, the oscillation is damped and for large distances  $q_{\text{eff}}$  becomes equal to  $q$ . This means that far away from the metal the dipoles are no longer influenced by the presence of the interface. This effect has already been described in the original work of CPS.<sup>5,6</sup> However, as we do not distinguish between plasmons and energy transfer from the dipoles to the metal electrodes in our simulations, the strong increase in  $q_{\text{eff}}$  for very short distances is mostly due to quenching effects.

#### D. Light extraction from OLEDs

We now use our simulation model to demonstrate how variations in the multilayer OLED stack given in Fig. 1 influence the light output from the device and the amount of power going into different loss channels. We note that this well-known structure, although not being particularly efficient, still serves as a model system for OLEDs with a single emitting material enclosed by a hole and an electron conducting compartment. This does also include phosphorescent emitters. Evidently, a strong influence on the amount of energy coupled into waveguided modes comes from the thickness of the various layers and the dipole layer position within the OLED stack. For the plasmonic modes the distance of the dipole layer to metallic electrodes is of great importance, as we will demonstrate below.

In Fig. 12 the dipole layer position is shifted successively from the cathode (Ca/Al interface) to the anode (PEDOT:PSS interface). This is achieved by fixing the overall thickness of the OLED, varying only the thicknesses of TPD and  $\text{Alq}_3$  accordingly. As their refractive indices are almost identical, this model shows the performance of the OLED if we could place the recombination zone arbitrarily within the

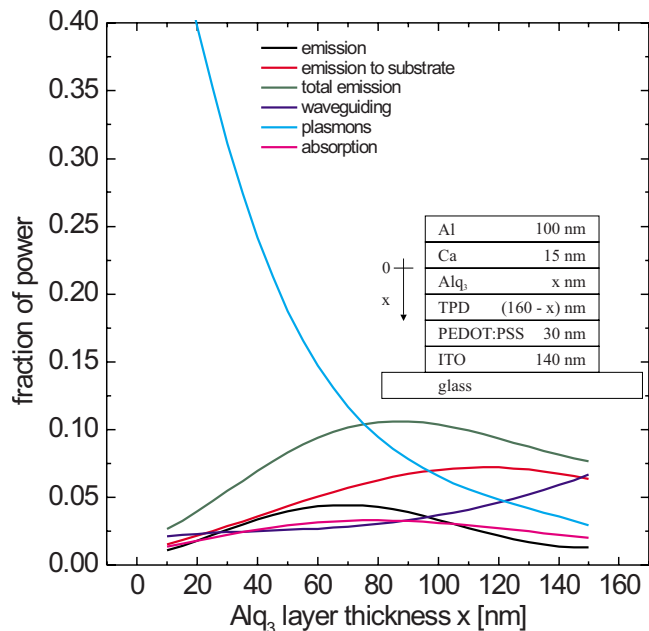


FIG. 12. (Color online) Variation in the dipole layer position. The overall thickness of the OLED is kept constant and the thicknesses of the  $\text{Alq}_3$  and TPD layer are varied accordingly. The dipole layer is located at the TPD/ $\text{Alq}_3$  interface and shifted from the Ca/Al cathode to the ITO anode. Radiative quantum efficiency  $q=0.2$ ,  $\Delta x=5$  nm.

organic layers (assuming that the electrical performance of the OLED is not affected). These similar refractive indices result in an almost constant absorption loss regardless of the dipole layer position. Most obvious, the plasmons are affected by the dipole layer position. Starting from the cathode a huge amount of power is coupled into plasmons. Moving farther away from the metal interface reduces this amount drastically. Therefore, the values for the direct emission and emission to substrate can increase. The direct emission reaches a maximum at an  $\text{Alq}_3$  layer thickness of about 70 nm. A further increase in the  $\text{Alq}_3$  thickness decreases this value again, which is due to the increasing amount of power coupled into waveguided modes. As a consequence of this simulation one can say that the recombination zone should not be placed too close to a metal interface due to the strong coupling to plasmons.

Changing the thickness of the hole transport layer at a fixed  $\text{Alq}_3$  thickness shows the influence of the waveguided modes on the emission of light, as can be seen in Fig. 13. The dipole layer has a fixed distance from the metallic cathode, resulting in an almost constant plasmon contribution. From an optical point of view the fraction of light coupled out directly has its maximum at small TPD layer thicknesses, whereas the amount of light going to the glass substrate has its maximum at a layer thickness where the waveguided modes have a minimum. This shows that the coupling to waveguided modes can be reduced to the benefit of light, which can leave the device through outcoupling structures; however the total amount of light (direct emission and emission to the substrate added together) would, from an optical point of view, suggest a preferably very thin TPD layer.

According to these results one could imagine that either the TPD layer should be avoided for optical reasons or that a

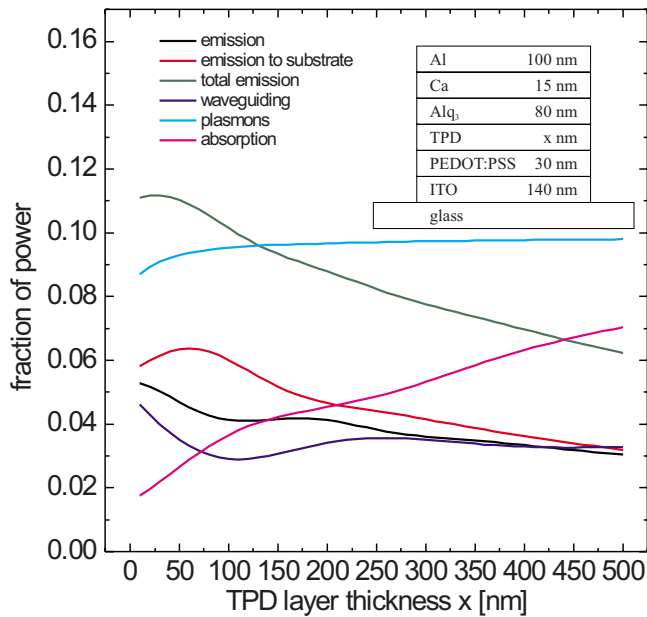


FIG. 13. (Color online) TPD layer thickness variation and radiative quantum efficiency  $q=0.2$ ,  $\Delta x=10$  nm.

shorter distance of the dipole layer to the anode could improve the fraction of light emitted from the OLED. For this reason we applied changes to the anode side of the ITO OLED stack: the PEDOT:PSS layer is omitted and the ITO thickness is reduced to 50 nm; the TPD layer thickness is still subject to variation. The results (not shown here) show a clear maximum (about 5.2%) for the direct emission at about 90 nm TPD layer thickness. Together with the previous simulation (Fig. 13), this leads to the conclusion that the TPD layer alone does not have a negative influence on the optical properties of the  $\text{Alq}_3$ -OLED stack, but that the distance of the dipole layer to the glass substrate is of importance.

The next simulations show the variation in the  $\text{Alq}_3$  layer thickness keeping the TPD layer fixed at 80 nm (Fig. 14). Here not only the layer thickness is changing, influencing the waveguided modes, but also the dipole position with respect to the cathode, resulting in a variation in the plasmon contribution. As the dipole layer is moved farther away from the cathode, the coupling to SPPs is reduced drastically. For the direct emission there exist several local maxima and minima as a function of distance. The first maximum at around 60 nm  $\text{Alq}_3$  layer thickness shows the highest fraction of out-coupled light (about 4.5%). This thickness (which at the same time is the distance of the dipole layer to the cathode) and also the value of the maximum external quantum efficiency of 1.1% [calculated from Eq. (8) with  $\gamma=1$  and  $\eta_{st}=0.25$ ] are consistent with the optimal thickness of  $\text{Alq}_3$  found in the experimental work.<sup>31–33</sup> However if outcoupling structures are attached to the OLED glass substrate the maximum fraction of totally outcoupled light (about 10.4%) is achieved with a slightly larger  $\text{Alq}_3$  layer thickness of about 80 nm.

As the thickness of  $\text{Alq}_3$  increases further a second maximum in the direct emission appears at 230 nm, which is slightly lower in value (about 3.8%) than the first maximum.

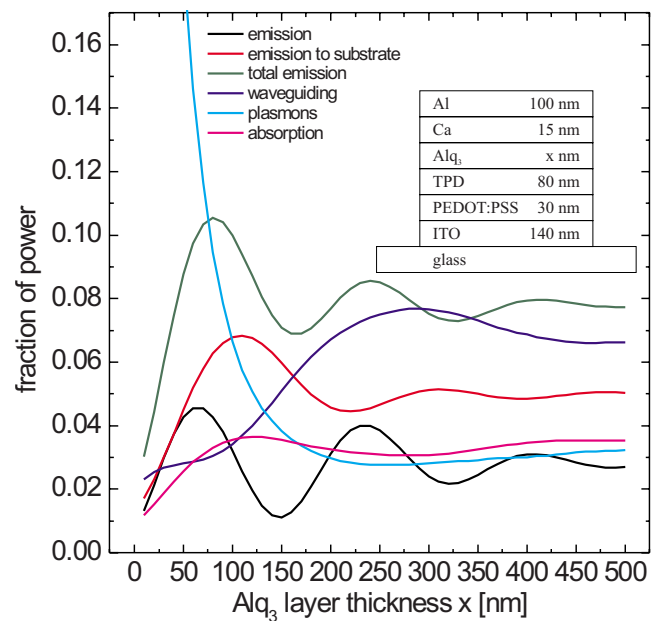


FIG. 14. (Color online)  $\text{Alq}_3$  layer thickness variation and radiative quantum efficiency  $q=0.2$ ,  $\Delta x=10$  nm.

Calculations where the radiative quantum efficiency is assumed to be  $q=1.0$  show that this second maximum can be even higher than the first one (Fig. 15). This effect has also been reported in literature.<sup>19</sup> OLED stacks with high quantum efficiency emitters therefore would benefit from an increased layer thickness on the cathode side of the emitter. Now the question arises why for emitters with small quantum efficiency this second maximum is lower than the first maximum for thinner layers. This behavior can be explained by the modification of the effective radiative quantum efficiency  $q_{\text{eff}}$  by the OLED cavity. As already shown in Fig. 11  $q_{\text{eff}}$  is enhanced especially at distances of the emitting dipole

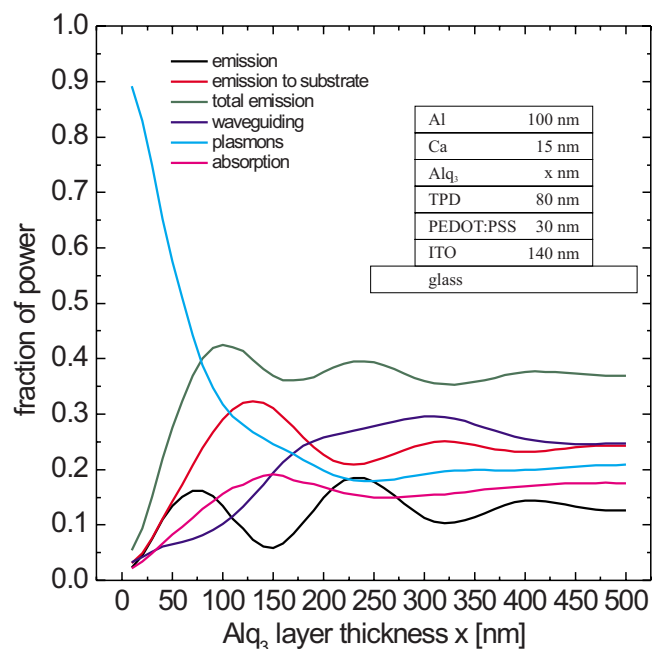


FIG. 15. (Color online)  $\text{Alq}_3$  layer thickness variation and radiative quantum efficiency  $q=1.0$ ,  $\Delta x=10$  nm.

to the metal electrode below 100 nm. This means that if the dipole is closer to the cathode ( $\approx 60$  nm) it gets amplified more as for larger distance ( $\approx 230$  nm), hence leading to a larger value for the fraction of directly emitted light in the first maximum in Fig. 14. However, as the direct emission is amplified for small distances, the amount of power coupled into the SPP also rises.

These simulations with different radiative quantum efficiencies  $q$  demonstrate that the value of  $q$  not only determines the amount of light that can be coupled out from an OLED but also the optimal layer thicknesses of the device. As a consequence the radiative quantum efficiency of the emitter in an OLED should be known for accurate device simulations and optimizations. In a forthcoming publication we will show that, if  $q$  is not known beforehand, simulations can be used to get access to its value by fitting the external quantum efficiency of devices with systematic layer thickness variations.

It should be noted that the optimizations of OLEDs presented here consider only the optical performance of the devices. Altering layer thicknesses will change the electrical properties, which have to be optimized as well. In this context, doped electron and hole transport layers will be important tools. Optimization of both the optical and electrical performance may require a compromise to be made; however this is not addressed in this work.

## V. SUMMARY

In conclusion, the simulations presented here show that the optical performance of OLEDs depends on several factors. Clearly the layer thicknesses of both the hole and the electron transport layers have a decisive influence. The dipole layer has to be located at the right position, so that the feedback exerted by the cavity on the emitting molecules is optimal for the fraction of light emitted directly or to the glass substrate and the fraction coupled to waveguided modes or SPPs is minimized. An important point is that the optimal dipole layer position (and thus the device structure) also depends on the radiative quantum efficiency  $q$  of the material used as emitter. Therefore this quantity has to be known for accurate device simulations and optimizations. Last, when optimizing the device it has to be considered if outcoupling structures will be used for the OLED, as the optimal layer thicknesses are slightly different to the ones for a plain OLED. Nevertheless, it is evident from these results that even in an optimized structure (with 100% radiative quantum efficiency) only some 40% of the radiation generated inside the OLED can actually be extracted, provided that all of the light guided as substrate modes could be

coupled out using suitable techniques. Further enhancement of the external OLED efficiency will therefore require the development of methods to couple out radiation from waveguided modes or even surface plasmons.

## ACKNOWLEDGMENTS

The authors would like to thank the German Federal Ministry of Education and Research (BMBF) for funding part of this work under Contract No. FKZ 13N8995 (OPAL).

- <sup>1</sup>T. Tsutsui, E. Aminaka, C. P. Lin, and D.-U. Kim, *Philos. Trans. R. Soc. London, Ser. A* **355**, 801 (1997).
- <sup>2</sup>C. W. Tang and S. A. VanSlyke, *Appl. Phys. Lett.* **51**, 913 (1987).
- <sup>3</sup>M. A. Baldo, D. F. O'Brien, Y. You, A. Shoustikov, S. Sibley, M. E. Thompson, and S. R. Forrest, *Nature (London)* **395**, 151 (1998).
- <sup>4</sup>H. Kuhn, *J. Chem. Phys.* **53**, 101 (1970).
- <sup>5</sup>R. R. Chance, A. Prock, and R. Silbey, *J. Chem. Phys.* **60**, 2744 (1974).
- <sup>6</sup>R. R. Chance, A. Prock, and R. Silbey, *Adv. Chem. Phys.* **37**, 1 (1978).
- <sup>7</sup>T. Tsutsui, C. Adachi, S. Saito, M. Watanabe, and M. Koishi, *Chem. Phys. Lett.* **182**, 143 (1991).
- <sup>8</sup>H. Becker, S. E. Burns, and R. H. Friend, *Phys. Rev. B* **56**, 1893 (1997).
- <sup>9</sup>N. C. Greenham, R. H. Friend, and D. D. C. Bradley, *Adv. Mater. (Weinheim, Ger.)* **6**, 491 (1994).
- <sup>10</sup>L. Novotny, *J. Opt. Soc. Am. A* **14**, 91 (1997).
- <sup>11</sup>W. L. Barnes, *J. Mod. Opt.* **45**, 661 (1998).
- <sup>12</sup>B. C. Krummacker, S. Nowy, J. Frischeisen, M. Klein, and W. Brütting (unpublished).
- <sup>13</sup>A. Sommerfeld, *Ann. Phys.* **333**, 665 (1909).
- <sup>14</sup>J. A. E. Wasey and W. L. Barnes, *J. Mod. Opt.* **47**, 725 (2000).
- <sup>15</sup>L. H. Smith, J. A. E. Wasey, I. D. W. Samuel, and W. L. Barnes, *Adv. Funct. Mater.* **15**, 1839 (2005).
- <sup>16</sup>K. Celebi, T. D. Heidel, and M. A. Baldo, *Opt. Express* **15**, 1762 (2007).
- <sup>17</sup>W. Lukosz and R. E. Kunz, *J. Opt. Soc. Am.* **67**, 1615 (1977).
- <sup>18</sup>C. Adachi, M. A. Baldo, M. E. Thompson, and S. R. Forrest, *J. Appl. Phys.* **90**, 5048 (2001).
- <sup>19</sup>C.-L. Lin, T.-Y. Cho, C.-H. Chang, and C.-C. Wu, *Appl. Phys. Lett.* **88**, 081114 (2006).
- <sup>20</sup>K. A. Neyts, *J. Opt. Soc. Am. A* **15**, 962 (1998).
- <sup>21</sup>B. Ruhstaller, T. Beierlein, H. Riel, S. Karg, J. C. Scott, and W. Riess, *IEEE J. Sel. Top. Quantum Electron.* **9**, 723 (2003).
- <sup>22</sup>N. A. Reinke, C. Ackermann, and W. Brütting, *Opt. Commun.* **266**, 191 (2006).
- <sup>23</sup>M. Cölle, J. Gmeiner, W. Milius, H. Hillebrecht, and W. Brütting, *Adv. Funct. Mater.* **13**, 108 (2003).
- <sup>24</sup>M. Cölle and W. Brütting, *Phys. Status Solidi A* **201**, 1095 (2004).
- <sup>25</sup>D. Z. Garbuzov, V. Bulović, P. E. Burrows, and S. R. Forrest, *Chem. Phys. Lett.* **249**, 433 (1996).
- <sup>26</sup>H. Mattoussi, H. Murata, C. D. Merritt, Y. Iizumi, J. Kido, and Z. H. Kafafi, *J. Appl. Phys.* **86**, 2642 (1999).
- <sup>27</sup>K. Meerholz and D. C. Müller, *Adv. Funct. Mater.* **11**, 251 (2001).
- <sup>28</sup>H. Kogelnik, in *Guided-Wave Optoelectronics*, edited by T. Tamir (Springer Verlag, Berlin, 1990).
- <sup>29</sup>W. Brütting, S. Berleb, and A. G. Mückl, *Org. Electron.* **2**, 1 (2001).
- <sup>30</sup>S. Nowy, N. Reinke, J. Frischeisen, and W. Brütting, *Proc. SPIE* **6999**, 69992V (2008).
- <sup>31</sup>S. K. So, W. K. Choi, L. M. Leung, and K. Neyts, *Appl. Phys. Lett.* **74**, 1939 (1999).
- <sup>32</sup>C. Schmitz, M. Thelakkat, and H.-W. Schmidt, *Adv. Mater. (Weinheim, Ger.)* **11**, 821 (1999).
- <sup>33</sup>T. A. Beierlein, Ph.D. thesis, University of Bayreuth, Germany, 2003.